Nanoscale

PAPER

View Article Online
View Journal | View Issue

Cite this: *Nanoscale*, 2017, **9**, 6076

Facile processes for producing robust, transparent, conductive platinum nanofiber mats†

Seongpil An,‡[a] Yong Il Kim,‡[a] Sumit Sinha-Ray,‡[b] Min-Woo Kim,[a] Hong Seok Jo,[a] Mark T. Swihart,[c] Alexander L. Yarin*[a,b] and Sam S. Yoon *[a]

Received 20th January 2017,
Accepted 18th April 2017

DOI: 10.1039/c7nr00479f

rsc.li/nanoscale

Mechanically robust freestanding platinum (Pt) nanofiber (NF) meshes are of great interest in applications where the corrosion resistance, malleability, and stability of a pure platinum structure must be combined with high surface area for catalysis. For photoelectrochemical applications, transparent electrodes are desirable. Several 1-dimensional (1D) Pt-based materials have been developed, but energy-intensive fabrication techniques and unsatisfactory performance have limited their practical implementation in next-generation photoelectrochemical applications. Here, we introduce relatively simple yet commercially-viable methods for creating robust, free-standing PtNF mats through combined electrospinning/solution blowing and electroplating steps. The PtNFs obtained by these processes exhibited outstanding low sheet resistance (R_s) values with reasonable transparency. In addition, the PtNFs were highly bendable and stretchable. Thus, the new methods and materials presented here hold great promise for creating mechanically robust and catalytically active transparent conducting films for diverse photoelectrochemical applications.

1. Introduction

Platinum is a noble metal of tremendous technological importance. It is used in a broad array of applications, including dye-sensitized solar cells (DSSCs),[1] photoelectrochemical (PEC) water splitting,[2] proton exchange membrane fuel cells (PEMFCs),[3] metal–air batteries,[4] sensors,[5,6] actuators,[7] exhaust gas purification,[8] and electrodes for neural stimulation.[9] In addition to unique catalytic activity for a wide variety of chemical reactions, Pt is known for its malleability, high temperature stability, and corrosion resistance. However, Pt is a rare metal (0.4 ng g^{-1} on Earth), being the 72nd most abundant element among 94 natural elements in the Earth's crust. The market price of Pt is accordingly very high (around 1000 US$/oz in 2016) and often exceeds that of gold.[10,11] Thus, efficient use of Pt is a key consideration across all of its many applications.

When Pt is purely used as a catalyst, its efficient use simply requires maximizing surface area by minimizing size. Thus, supported Pt catalysts use highly-dispersed nanoparticles, or even individual Pt atoms on a high-surface-area support material.[10] However, in many applications, other properties of Pt including mechanical strength, corrosion resistance, and electrical conductivity are essential. In those cases, structures of pure, unsupported Pt are needed. To address such needs, numerous researchers have sought to create pure Pt structures with a high surface-area-to-volume ratio (S/V) by using nano- or micro-scale fabrication techniques. Notably, structures composed of 1-dimensional (1D) Pt materials, such as Pt nanowires (PtNWs), Pt nanotubes (PtNTs), and Pt nanofibers (PtNFs), exhibit reasonably enhanced performance due to their anisotropic structure with a high S/V (Table S1†). However, the mechanical stability of many of these structures has been unsatisfactory. In addition, most published approaches require complicated fabrication processes, thereby making their future applicability quite uncertain. For example, Kim *et al.*[12] recently developed PtNF webs with low sheet resistance (R_s = 40 Ω sq^{-1}) with a transmittance (T) of 68%. More recently, Chen *et al.*[13] developed copper (Cu)–Pt core–shell NWs with R_s = 38 Ω sq^{-1} and T = 83.4%. Low sheet resistance in such structures reflects strong interconnections between individual NWs or fibers, which also benefits mechanical properties. Light transmission is essential in applications such as DSSCs. However, the previously reported Pt structures and processes still have substantial limitations, such as the energy-consuming thermal post-treatment and multi-step fabrication processes and performance limitations caused by the presence

[a]*School of Mechanical Engineering, Korea University, Seoul 02841, Republic of Korea. E-mail: ayarin@uic.edu, skyoon@korea.ac.kr*
[b]*Department of Mechanical and Industrial Engineering, University of Illinois at Chicago, 842 W. Taylor St., Chicago, IL 60607-7022, USA*
[c]*Department of Chemical & Biological Engineering, University at Buffalo, The State University of New York, Buffalo, New York 14260-4200, USA*

†Electronic supplementary information (ESI) available. See DOI: 10.1039/c7nr00479f

‡These authors contributed equally to this work.

of other elements in addition to Pt. These limitations may restrict their practical implementation, and thus improved methods of production of pure Pt nanostructures with low sheet resistance, robust mechanical properties, and high light transmittance, along with the inherent catalytic activity and corrosion resistance of Pt, are still needed.

Herein, we demonstrate a novel method for fabricating translucent, flexible, high-purity platinum nanofiber (PtNF) mats by combining electrospinning/solution blowing and electroplating methods; this approach is simple, low-cost, scalable, and commercially-viable. Very low R_s values were achieved in combination with reasonable transparency. Thus, the present approach holds great promise as a step toward realizing a commercially-viable catalytic material for applications such as DSSCs where mechanically-robust, corrosion-resistant and electrocatalytically active Pt structures are needed.

2. Experimental

2.1 Materials

Polyacrylonitrile (PAN, M_w = 150 kDa) and *N*,*N*-dimethylformamide (DMF, 99.8%) were obtained from Sigma-Aldrich (USA). A chloroplatinic acid solution (H_2PtCl_6, 5 wt% in distilled water), platinum (Pt)-frames, and Pt-plates were obtained from HanTeck PMC (Gyeonggi-do, Republic of Korea). To prepare polyvinylpyrrolidone (PVP, M_w = 40 kDa)-aluminum acetate (AlAc) nanofibers (NFs), PVP, AlAc and the solvent (formic acid) were purchased from Sigma-Aldrich (USA). Chloroplatinic acid hydrate, used for further Pt plating, was also obtained from Sigma-Aldrich. A Pt/Pd (80/20) disk was provided by the Research Resource Center, UIC, as a source for platinum plating.

2.2 Polymer nanofibers

First, 8 wt% PAN solution was prepared by dissolving PAN in DMF and stirring for one day at room temperature. Next, the homogeneous PAN solution was supplied through a syringe equipped with an 18-gauge needle (Nordson EFD, USA). The flow rate of the solution was fixed at Q = 250 μL h^{-1} by adjusting the syringe pump (Legato 100, KD Scientific Inc., USA). Simultaneously, a high DC voltage of V = 7.5 kV was applied to the needle for formation of the Taylor cone using a DC power supply (EP20P2, Glassman High Voltage Inc., USA). The polymer jet from the supercritical Taylor cone was electrospun. As usual, electrically-driven bending instability of the polymer jet set in,[14,15] which resulted in ultra-thin fibers in the range of hundreds of nm in diameter. The NFs were deposited onto the Pt-frame to obtain free-standing NFs and the electrospinning time was 90 s. The needle-to-collector distance was 14 cm.

In the second method used in this study, two separate procedures were followed. First, PAN NFs were formed *via* electrically-assisted subsonic solution blowing. A 6 wt% PAN solution in DMF was used to blow the PAN NFs with diameters in the range of ~100–300 nm *via* solution blowing. The polymer solution was pumped through a 25-gauge needle at a flow rate of 0.3 mL h^{-1} using a syringe pump (New Era Pump Inc., USA). The needle was connected to a high voltage supply where the ground was a Laval nozzle placed normal to the electrospinning needle. The pressure of the air supplied through the Laval nozzle was kept at 20 psi, which is different from that in our previous study,[16] where a similar approach was used but the air pressure was 70 psi. The applied voltage was 5.6 kV. The polymer jet issued from the nozzle, was pulled by the electric forces to the Laval nozzle where it was swept away by the strong air flow. The polymer jet experienced electrically-driven and then aerodynamically-driven bending instability and thinned down to ~100–300 nm in diameter. The NFs were collected over an aluminium (Al) wire frame with dimensions of 1 cm × 1 cm for 15 min to obtain a sufficiently thick NF mat. The NFs were then glued onto the edges of the wire frame with a water insoluble adhesive (a spirit gum) for better adhesion during subsequent processing steps.

To produce alumina NFs, PVP-AlAc NFs were first formed by electrospinning using a blend of two solutions. To prepare the solutions, 2 g of PVP was dissolved in ethanol, and 2 g of aluminum acetate was dissolved in a mixed solvent comprised of DI water and formic acid in a 3 : 1 ratio. The AlAc-formic acid–DI water mixture was sonicated in a bath sonicator for 2 h, while the PVP-ethanol solution was kept on a magnetic stirrer for 6 h at 45 °C. After the AlAc solution became clear, it was mixed with the PVP solution and magnetically stirred at 45 °C for a further 6 h period. The mixture was then electrospun to form PVP-AlAc NFs. To accomplish this, the mixed solution was pumped through an 18-gauge needle at a flow rate of 0.8 mL h^{-1} using a syringe pump. The applied electrical potential was 16 kV and the needle-to-collector distance was 15 cm. The collector was a rotating disk with a width of 2.5 cm, rotating at 220 rpm. The NFs were collected for 6 h to create a sufficiently thick NF mat. The collected PVP-AlAc NFs were then calcined in a furnace at 600 °C for 6 h in air to eliminate the polymer and obtain alumina NFs.

2.3 Platinum nanofibers

The Pt-electroplating solution (500 mL) was obtained by diluting 80 mL of 5% H_2PtCl_6 solution with 420 mL of DI water. The solution was magnetically stirred for 24 h at room temperature to stabilize the solution. The pH was readjusted to pH = 1.5 by adding sulfuric acid (H_2SO_4) or sodium hydroxide (NaOH). Prior to electroplating the polymer NFs, the free-standing PAN NFs were sputtered with a Pt (MSP-1S, Vacuum Device Inc., Japan) layer a few nm thick, which facilitated electroplating of the initially non-conductive polymer NFs. Note that it is also possible to sputter NFs with gold (Au).

Electroplating was carried out using a simple two-electrode setup at room temperature in air. A Pt-plate (3 × 3 cm^2) was used as the working electrode (anode) and the Pt-frame (where the free-standing PAN NFs were suspended) was used as the counter electrode (cathode). The electrical current density during electroplating was fixed at 0.11 A cm^{-2} by using a power supply (SPS-1820, GW Instek, Taiwan). The distance

between the electrodes was 2 cm. The electroplating time (t_e) was varied from 15 to 90 min.

In the second method used in the present work, both PAN and ceramic (alumina) NFs were sputter-coated with 8 nm of Pt/Pd on both sides using a Cressington sputter coater. It should be emphasized that the thin layer of adhesive that was applied at the edges of the frame was also sputter-coated and thus became conductive, which facilitated establishment of a proper electrical connection for the ensuing Pt-plating process. The electroplating solution comprised a 5 mM H_2PtCl_6 solution in 100 mL of DI water. A Pt-plate (1 cm width and 2 cm height) was used as the anode and the substrates were used as the cathode. The NFs were then plated with Pt for t_e = 15 min in the HSEPS-10 electroplating station under an electric current density of ~200 mA cm^{-2}. The electrodes were kept at a distance of 4 cm. The high current density allowed formation of a "bumpy" coating on the NFs, as revealed in the SEM images.

2.4 Characterization

The morphologies of the NF mats were observed using field-emission scanning electron microscopy with energy dispersive X-ray spectroscopy (FE-SEM/EDX, Quanta 250 FEG, FEI). The average diameter (D_{avg}) of the NFs was evaluated by analysis of 100 NFs from the SEM images. Qualitative analyses of the PtNFs were conducted by X-ray diffraction (XRD, SmartLab, Rigaku) and X-ray photoelectron spectroscopy (XPS, X-tool, ULVAC-PHI). The cross-sectional structure of the PtNFs was evaluated using a transmission electron microscope (TEM, JEM 2100F, JEOL Inc.). The sample for TEM analysis was prepared by using a dual beam focused ion beam (FIB, LVRA3 XMH, TESCAN). The transmittance and sheet resistance values were obtained by UV-VIS spectrophotometry (Optizen POP, Mecasys) and using a sheet resistance meter (FPP-400, Dasol Eng), respectively. Note that air was used as a reference (background) for the transmittance measurement. The photoelectrochemical current densities (PCD) were measured by using a chemical reactor with three electrodes. Bismuth vanadate ($BiVO_4$) and Ag/AgCl were used as a working and a reference electrodes, respectively.[17] The electrolyte solution was a 0.5 M Na_2SO_4 (pH = 7). A Xe arc lamp (Newport, Oriel Instruments) equipped with an AM 1.5 filter was used as an irradiation source, yielding a light intensity of 100 mW cm^{-2}. The PCD values were recorded by a potentiostat (VersaSTAT-3, Princeton Applied Research) with a scan rate of 10 mV s^{-1} in the applied voltage range of 0.0–1.2 V *vs.* Ag/AgCl.

The solution-blown PAN NFs and electrospun ceramic NFs were observed using a field-emission scanning electron microscope (JEOL-JSM 6320F, RRC, UIC). The X-ray diffraction pattern of the platinum coating on such NFs was studied using a Siemens (Bruker) D-5000 Powder Diffractometer.

3. Results and discussion

High-purity platinum nanofibers (PtNFs) were fabricated by a combination of electrospinning and electroplating, as illustrated in Fig. 1. Prior to electroplating (Fig. 1a), polyacrylonitrile (PAN) NFs were deposited on a Pt-frame as translucent, free-standing NF mats (Fig. S1a†). The details of the electrospinning conditions can be found in the Experimental section.

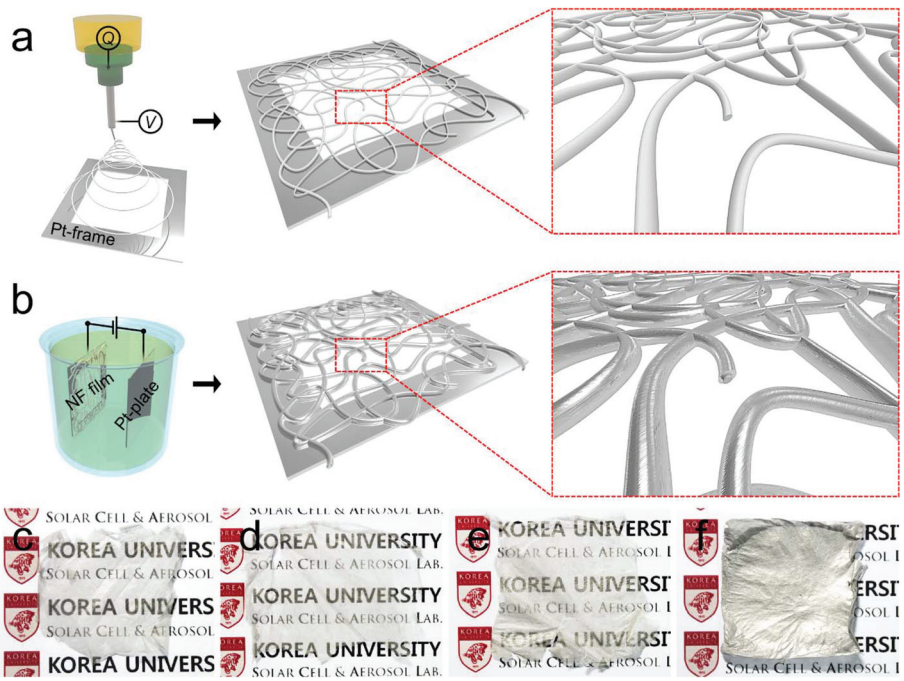

Fig. 1 Schematic of the process for fabrication of the (a) electrospun PAN NFs on the Pt-frame and (b) the electroplated PtNFs on the Pt-frame, and photographs of the PtNF mats formed at different electroplating times, t_e: (c) t_e = 15 min, (d) t_e = 30 min, (e) t_e = 45 min, and (f) t_e = 90 min.

Uniformly electrospun NFs with an average diameter (D_{avg}) of 530 nm, were obtained (Fig. S2†). The outer surface of the PAN NFs was then seeded with metal nanoparticles *via* sputtering (see Fig. S1b† and the Experimental section for details). These metal nanoparticles trigger the initial electroplating, thereby facilitating Pt-plating of the non-conductive PAN NFs. The metal-seeded NF mat was electroplated in a chloroplatinic acid solution (H_2PtCl_6, Fig. 1b; see the Experimental section for details).

Fig. 1c–f show the PtNF mats fabricated using electroplating times (t_e) from 15 to 90 min. Metallic-colored translucent PtNF mats were obtained, except in the case of t_e = 90 min, which produced an opaque mat. These translucent materials are particularly attractive for future use in photoelectrochemical applications.[13,18,19] Light transmission at 550 nm (T_r) decreased with increasing t_e, from 55% for t_e = 15 min to 7% for t_e = 90 min (Fig. S3† and Table 1). Note that T_r of the PAN NF mat was 81%. To better characterize the PtNF mats, SEM analysis was conducted as shown in Fig. 2. Smoothly-plated PtNFs were obtained for t_e = 15 and 30 min, whereas slightly-roughened PtNFs were obtained for t_e = 45 and 90 min (*cf.* Fig. S4†). This nano-textured surface may be generated due to crystallization during the Pt-coating process.[20]

Table 1 Transmittance at λ = 550 nm and sheet resistance values for the PtNF mats

Case	Experimental result			Percolation model		
t_e (min)	D_{avg} (nm)	T_r (%)	R_s (Ω sq^{-1})	R	p	b
15	642	55	14.1	1.8	0.7055	0.1276
30	821	48	4.32	1.8	0.7130	0.1459
45	1220	36	0.88	1.4	0.8068	0.1587
90	2483	7	0.15	—		

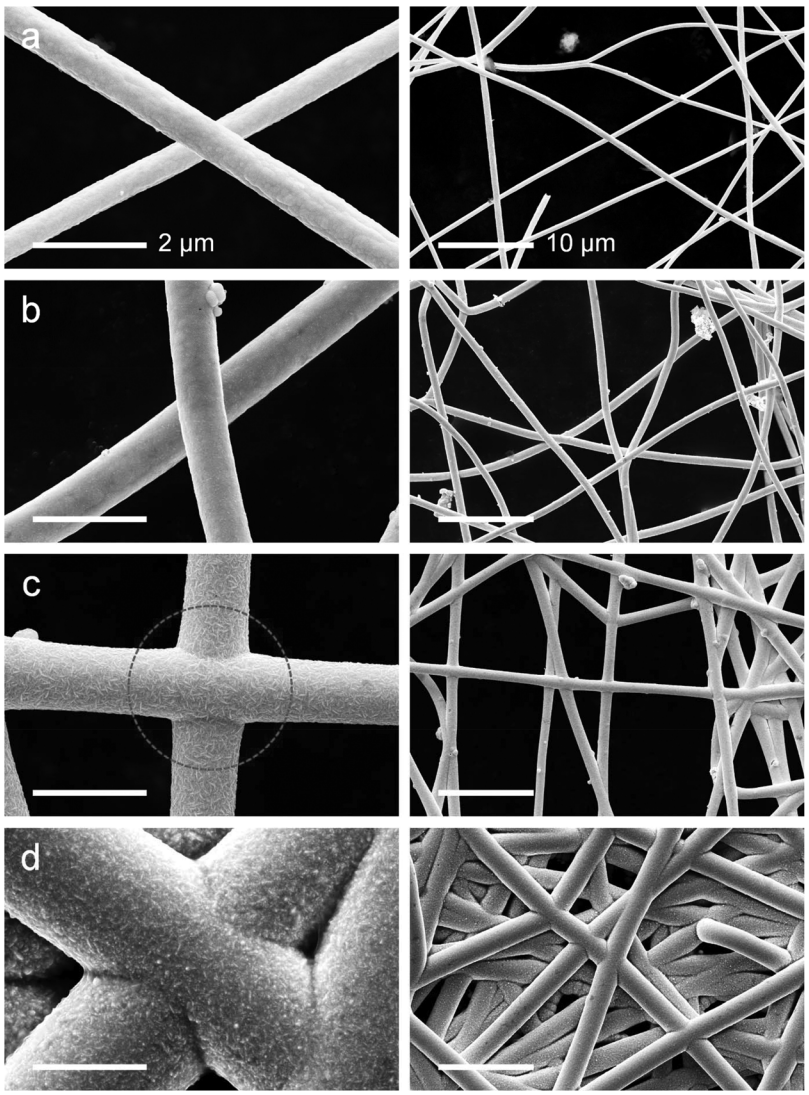

Fig. 2 SEM images of the PtNF mats fabricated using different values of t_e: (a) t_e = 15 min, (b) t_e = 30 min, (c) t_e = 45 min, (d) t_e = 90 min. The inset scale bars in each column are the same.

Starting from t_e = 45 min, the junctions between NFs were completely connected, leading to a dramatic reduction of the electrical contact resistance at the fiber junctions.[21] The sharp decrease in sheet resistance after t_e = 45 min shows that there is threshold time for complete fusion of the junctions. Accordingly, after t_e = 45 min, the sheet resistance (R_s) decreased significantly to below 1 Ω sq^{-1}. Increasing the t_e from 15 to 90 min decreased R_s of the PtNF mats by two orders of magnitude, from 14.1 to 0.15 Ω sq^{-1} (Table 1). The D_{avg} value of the PtNFs increased from 642 to 2483 nm as the t_e increased from 15 to 90 min (Table 1), in particular, a multi-layered structure was obtained at t_e = 90 min (Fig. 2).

Qualitative analysis of the PtNF mat *via* XRD and XPS analyses was performed using the mat formed at t_e = 45 min (Fig. 3a and b). The XRD profile (Fig. 3a) confirmed the presence of high-purity Pt. The peaks at 2θ = 40.4°, 46.9°, and 68.2° respectively correspond to the (111), (200), and (220) planes of face-centered cubic (fcc) Pt (JCPDS no. 87-0647). Fig. 3b shows the high-resolution Pt 4f XPS spectrum, where the two main peaks at 70.9 and 74.1 eV are assigned to Pt 4f$_{7/2}$ and Pt 4f$_{5/2}$, respectively.[22] In addition, elemental mapping by energy-dispersive X-ray spectroscopy (EDX) combined with SEM images of the PtNF mats (Fig. 3c–f) confirmed the presence of Pt on the PAN NF surfaces. To further characterize a single PtNF, a cross-section of a single PtNF was obtained by focused ion beam (FIB) milling (Fig. S5†).[23] Cross-sectional TEM images of the PtNF in Fig. 4a and b clearly show a core–shell structure. The core diameter and the shell thickness in the horizontal direction were 455 and 542 nm, respectively. These values are slightly smaller than the average values (*cf.* Table 1). It seems that there is no PAN NF at the core, resulting in a doughnut-like morphology (*cf.* Fig. 4b). However, we cannot conclude whether the NF was removed in the electroplating process or during the FIB milling process. The elemental mapping TEM image in Fig. 4c also confirmed the complete formation of a Pt shell. Furthermore, the selected area electron diffraction (SAED) pattern in Fig. 4d revealed that the shell part of the PtNF consisted of fcc Pt with the space-group $Fm\bar{3}m$.[24]

Fig. 5 illustrates the robust mechanical properties of the PtNF mat obtained at t_e = 45 min. The remarkably low sheet resistance (R_s = 0.88 Ω sq^{-1}) enabled operation of six LED lamps without any significant light loss (Fig. 5a). In the bending test (Fig. 5b), the PtNF mat maintained its initial conductivity without significant degradation even after 2000 cycles ($R/R_0 \sim 1$), which indicates high flexibility of the PtNF mat. Breakage of individual NFs or separation of NF junctions would have produced an increase in resistance. In the stretching tests (Fig. 5c and d, and Movie S1†), even though gradual electrical degradation was observed as the strain increased up to 400% (Fig. 5c) and the repetitive stretching was conducted up to 90 cycles (Fig. 5d, where the strain was 200%), the available stretchability was comparable to those previously reported for TCEs.[25,26] The PtNF mats were transferred onto PET and Eco-flex mats for the bending and stretching tests, respectively.

To assess the catalytic activity of the PtNF mat, the catalytic performance in photoelectrochemical (PEC) water splitting was studied as shown in Fig. 6 and in Table S1.† Increasing the electrode surface area in water splitting is a key factor to enhance PEC performance, which has been considered as one of the most challenging issues in photocatalytic application studies.[17,27–30] To use the PtNF mat as a counter-electrode for the PEC measurement, the rolled-up PtNF mat (t_e = 60 min) was prepared and then installed in a 2 mL Vycor frit (Princeton Applied Research, *cf.* inset images in Fig. 6). Both the rolled-up PtNF mat and a commercial Pt electrode (K0266, Princeton Applied Research) were examined for comparison in the PEC water splitting tests. The obtained photocurrent

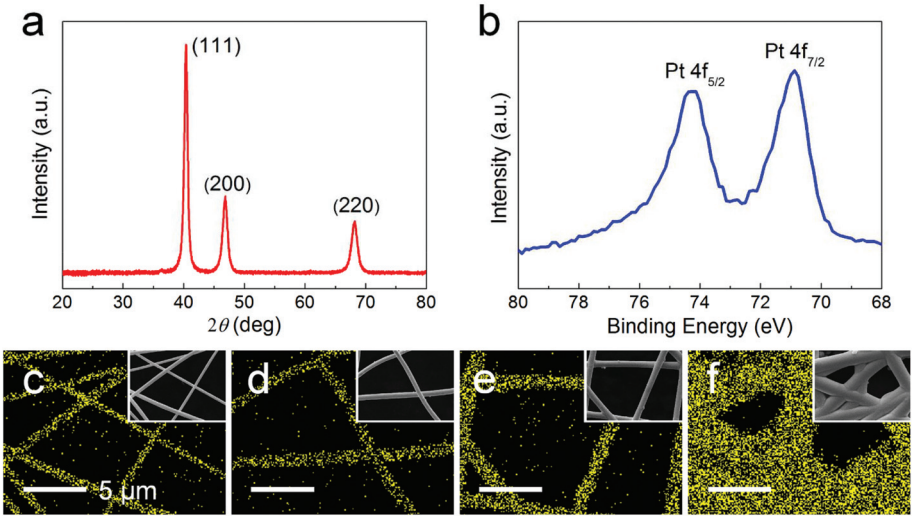

Fig. 3 (a) XRD and (b) high-resolution XPS spectra for the PtNF mat prepared with t_e = 45 min. Elemental mapping SEM/EDS images of the PtNF mats as a function of t_e: (c) t_e = 15 min, (d) t_e = 30 min, (e) t_e = 45 min, (f) t_e = 90 min. Inset scale bars are the same.

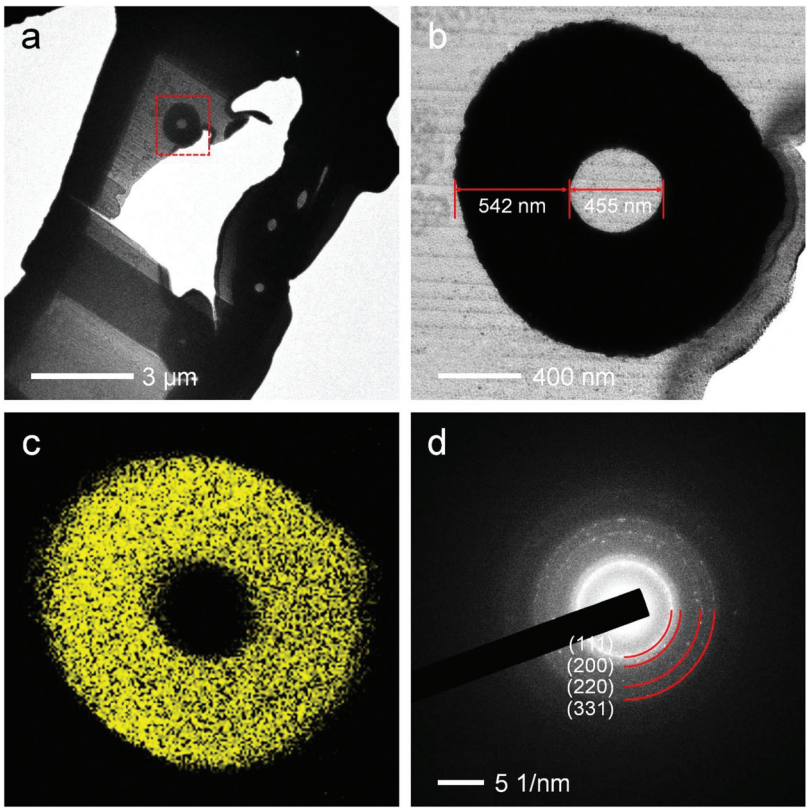

Fig. 4 (a, b) Cross-sectional and (c) elemental mapping TEM images of the FIB-treated PtNF sample (t_e = 45 min). (d) SAED pattern of the corresponding PtNF.

density (PCD, at 1.2 V *vs.* Ag/AgCl) by the PtNF mat was 1.17 mA cm^{-2}, whereas that of the commercial Pt electrode was 1.10 mA cm^{-2}. It should be emphasized that the higher PCD value of the PtNF mat was achieved by using only one-fifteenth amount (by weight) of the commercial Pt electrode. Specifically, the weight of the tested PtNF mat was 0.035 g, whereas that of the commercial Pt electrode was 0.51 g. The high surface area of the PtNF mat, which originates from the unique 1-dimensional (1D) NF structure, facilitated a high PCD value comparable to that of the expensive commercial Pt electrode. Such an impressive PEC performance demonstrates distinctly that the PtNF mat holds potential for various PEC applications.

It should be emphasized that a high T_r could be achieved for the PtNF mat by reducing the amount of electrospun PAN NFs; however, this inevitably increased the R_s. When a short electrospinning time of 30 s was employed (Fig. S6†), a higher T_r (80%) was obtained than that achieved with a long electrospinning time (T_r = 36%, see Table 1), where the R_s obtained for the short electrospinning time was higher (R_s = 8.3 Ω sq^{-1}) than that achieved with the long electrospinning time (R_s = 0.88 Ω sq^{-1}). Note that the value of t_e was the same (t_e = 45 min) in both cases.

Electrically-assisted solution blowing produced even smaller PAN NFs, allowing production of smaller diameter PtNFs. The solution-blown PAN NFs were completely covered with Pt, as shown in Fig. 7a. A higher-zoom view of a Pt grain is also highlighted in Fig. 7a; the size of the grain is about 70 nm. During the electroplating process, the voltage was kept constant at 4 V, and because the electrode distance was sufficiently large, the offset voltage did not increase, which eliminated thicker preferential coating at the edges. Pt-plating for 15 min was sufficient to achieve even Pt deposition on the NFs. The X-ray diffraction pattern acquired in the 2θ range of 20–80° also confirmed the presence of Pt on the NFs (Fig. S7†). Characteristic peaks were observed at 2θ angles of 39.98°, 46.2°, and 67.4°, corresponding to the (111), (200), and (220) crystal planes with respective *d*-spacings of 2.255 Å, 1.961 Å, and 1.386 Å. These values closely match the standard X-ray diffraction pattern of pure Pt.[31] This confirms the presence of pure Pt on the NFs. It should be emphasized that Pt oxidation at room temperature is very difficult because Pt is a noble metal, the oxide of which is less stable than the metal and lies in the endothermic region of the Ellingham diagram.[32] Similar features were also observed for the Pt-coated alumina fibers, for which a rough and "bumpy" Pt coating was readily visible in the SEM images (*cf.* Fig. 7b).

In addition to the experimental features discussed above, theoretical analysis was performed using the percolation model introduced in our previous study.[21] It should be empha-

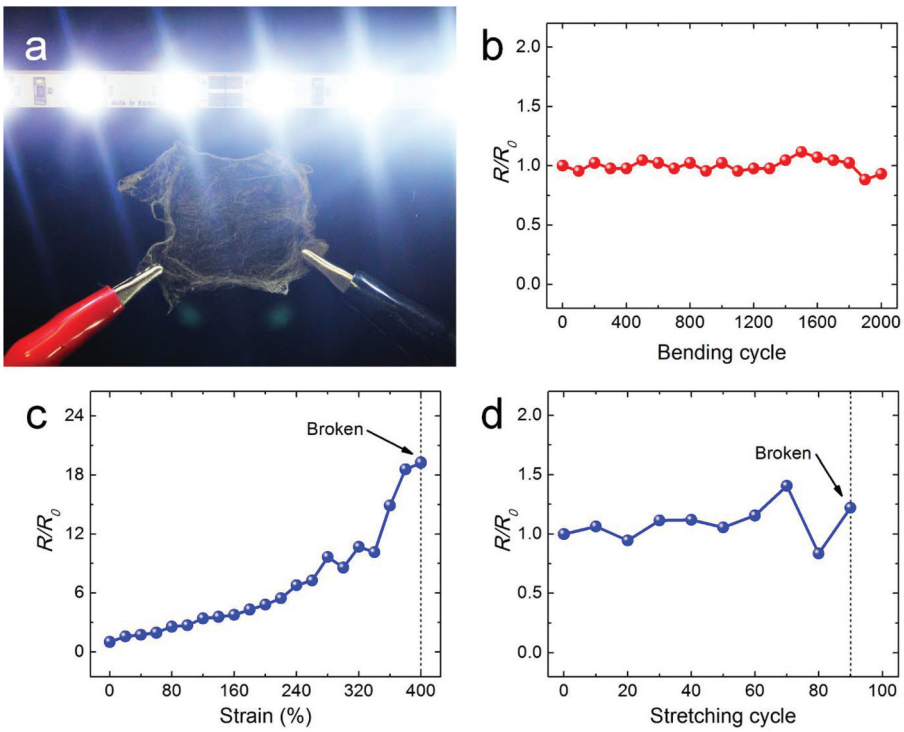

Fig. 5 (a) Photograph of LED operation and fatigue study data of the PtNF mat (t_e = 45 min): (b) bending cycle, (c) tensile test, and (d) stretching cycle.

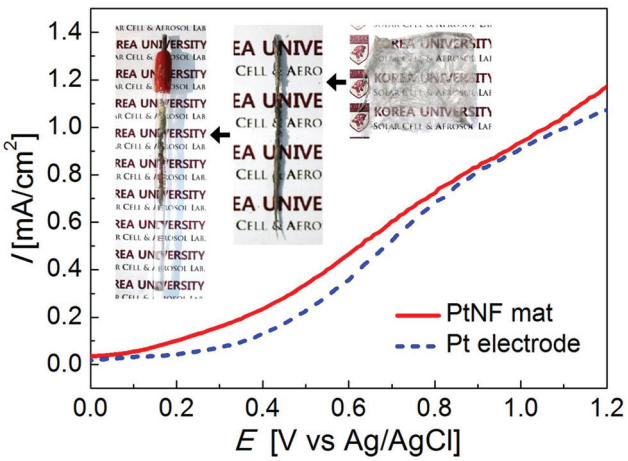

Fig. 6 *I–V* curves for the rolled-up PtNF mat (t_e = 60 min) and the commercial Pt electrode. Insets are photographs for the rolled-up PtNF mat.

sized that this percolation model is based on the classical percolation theory,[33,34] and thus allows analytical explanation of the experimental behavior of R_s and T_r of 1D material-based TCEs, especially NF-based TCEs.

Two important parameters for assessment of the NFs are the probability, p (which indicates the probability of self-junctioned PtNFs) and the shading factor, b (which is related to the diameter of a single PtNF). Then, the following two equations were obtained *via* the renormalization-group technique of the classical percolation theory:[21]

$$C = \frac{11}{3}p^3(1-p)^2 + p^2(1-p)^3 + \frac{17}{5}p^4(1-p) + p^5 \quad (1)$$

$$T = 1 - 5b[p(1-p)^4 + 4p^2(1-p)^3 + 6p^3(1-p)^2 + 4p^4(1-p) + p^5] = 1 - 5bp \quad (2)$$

Here, C is the expected normalized conductivity and T is the predicted transmittance. When a percolating cluster becomes larger ($p \rightarrow 1$), C becomes close to the intrinsic conductivity of an individual PtNF ($C \rightarrow 1$). In contrast, in a rarefied non-percolating cluster ($p \rightarrow 0$), the value of C tends to nil. A more detailed explanation of eqn (1) and (2) can be found in ref. 21.

The p values of the PtNF mats were determined by substituting the corresponding dimensionless R (= $1/C = R_{single}/R_s$) values (Table 1) into eqn (1). Here, R_{single} is the numerically-calculated resistance of a single PtNF, which is defined as $R_{single} = \rho L/A$. The resistivity of Pt is $\rho = 1.06 \times 10^{-7}$ Ω m. The average length between the fiber intersections (L) and the cross-sectional area (A) of the PtNFs was obtained by analysis of 100 NFs from the SEM images (*cf.* Fig. 3); the average length differed for the various cases (Table S2†). Using both the obtained p values from eqn (1) and the experimental values of T ($T = T_r/100$), the b values were determined using eqn (2), as listed in Table 1. For example, b = 0.1276 was obtained for the t_e = 15 min case by substituting both p = 0.7055 and T = 0.55

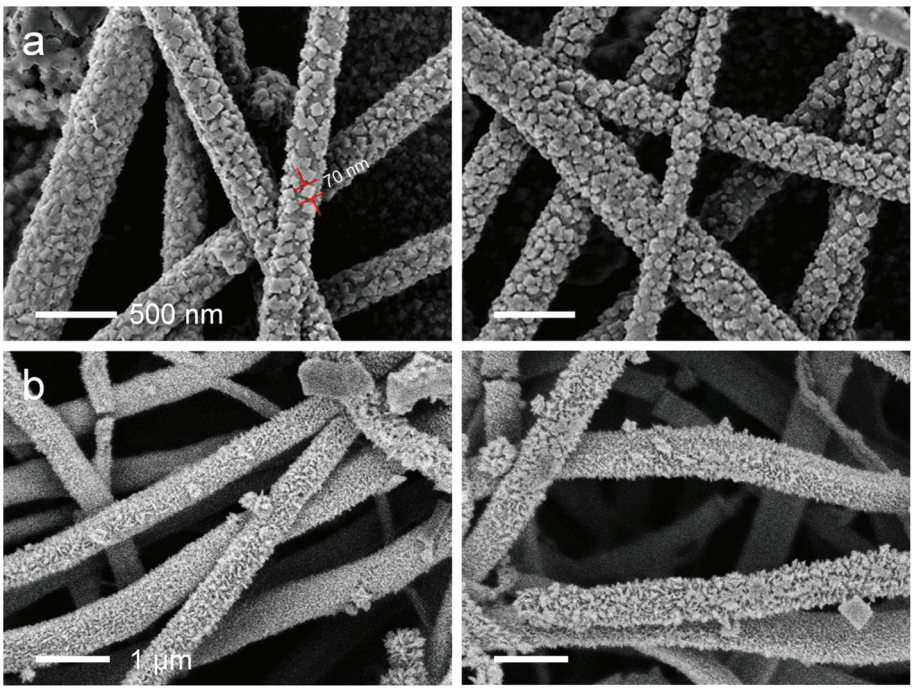

Fig. 7 (a) SEM images of PtNFs obtained by electrically-assisted solution blowing of 6 wt% PAN solution in DMF. An individual crystal of Pt (size 70 nm) is highlighted in panel (a). (b) SEM images of Pt-plated alumina NFs.

into eqn (2). It is impossible to apply this percolation model to the multi-layered structure corresponding to the t = 90 min case (*cf.* Fig. 2d) because the percolation model is based on 2-dimensional bond lattices, corresponding to a single-layered NF structure. The p and b values both increased as t_e increased (conversely, R_s decreased). It was found that the p value should be higher than ~0.8 to obtain an R_s value lower than ~1 Ω sq^{-1} for NF-based TCEs by comparing our previous[21] and present results. The self-junction phenomenon occurs for the NFs when the p values are greater than ~0.8. Even though the b value may be high, the p value is low when there is little self-junctioning of the NFs. For example, the PtNF mat prepared with an electrospinning time of 30 s (*cf.* Fig. S6†) had a high b value of 0.1477. However, the p value was very low (0.2709) and a weak self-junction effect was observed, as shown in the SEM images (Fig. S6c†).

4. Conclusion

A facile new method for fabrication of free-standing platinum nanofiber (PtNF) mats *via* electrospinning/solution blowing combined with electroplating was demonstrated. The translucent PtNF mats exhibited excellent sheet resistance (R_s) values with exceptional mechanical properties. The low sheet resistance was attributed to elimination of junction resistance at NF intersections due to conformal coating during the electroplating process. In addition, the percolation parameters for achieving performance-enhanced transparent conducting electrodes (TCEs) were examined. These novel PtNF mats hold great promise for various photoelectrochemical applications.

Acknowledgements

This research was supported by National Research Foundation of Korea (NRF-2017R1A2B4005639) and Global Frontier Program through the Global Frontier Hybrid Interface Materials (GFHIM) of the National Research Foundation of Korea (NRF) funded by the Ministry of Science, ICT & Future Planning (2013M3A6B1078879) and the Technology Development Program to Solve Climate Changes of the National Research Foundation (NRF-2016M1A2A2936760).

References

1 A. Hagfeldt, G. Boschloo, L. Sun, L. Kloo and H. Pettersson, *Chem. Rev.*, 2010, **110**, 6595–6663.
2 M. G. Walter, E. L. Warren, J. R. McKone, S. W. Boettcher, Q. Mi, E. A. Santori and N. S. Lewis, *Chem. Rev.*, 2010, **110**, 6446–6473.
3 S. Sun, G. Zhang, D. Geng, Y. Chen, R. Li, M. Cai and X. Sun, *Angew. Chem., Int. Ed.*, 2011, **123**, 442–446.
4 Y.-C. Lu, Z. Xu, H. A. Gasteiger, S. Chen, K. Hamad-Schifferli and Y. Shao-Horn, *J. Am. Chem. Soc.*, 2010, **132**, 12170–12171.
5 S. Guo, D. Wen, Y. Zhai, S. Dong and E. Wang, *ACS Nano*, 2010, **4**, 3959–3968.

6 Y. Yuan, R. T. Kwok, B. Z. Tang and B. Liu, *J. Am. Chem. Soc.*, 2014, **136**, 2546–2554.
7 H.-J. Jin, X.-L. Wang, S. Parida, K. Wang, M. Seo and J. Weissmüller, *Nano Lett.*, 2009, **10**, 187–194.
8 H. Koga, Y. Umemura, A. Tomoda, R. Suzuki and T. Kitaoka, *ChemSusChem*, 2010, **3**, 604–608.
9 S. F. Cogan, *Annu. Rev. Biomed. Eng.*, 2008, **10**, 275–309.
10 A. Bruix, Y. Lykhach, I. Matolínová, A. Neitzel, T. Skála, N. Tsud, M. Vorokhta, V. Stetsovych, K. Ševčíková and J. Mysliveček, *Angew. Chem., Int. Ed.*, 2014, **53**, 10525–10530.
11 F. Reith, S. G. Campbell, A. S. Ball, A. Pring and G. Southam, *Earth-Sci. Rev.*, 2014, **131**, 1–21.
12 J. Kim, J. Kang, U. Jeong, H. Kim and H. Lee, *ACS Appl. Mater. Interfaces*, 2013, **5**, 3176–3181.
13 Z. Chen, S. Ye, A. R. Wilson, Y.-C. Ha and B. J. Wiley, *Energy Environ. Sci.*, 2014, **7**, 1461–1467.
14 D. H. Reneker, A. L. Yarin, H. Fong and S. Koombhongse, *J. Appl. Phys.*, 2000, **87**, 4531–4547.
15 A. L. Yarin, B. Pourdeyhimi and S. Ramakrishna, *Fundamentals and Applications of Micro-and Nanofibers*, Cambridge University Press, 2014.
16 S. Sinha-Ray, M. W. Lee, S. Sinha-Ray, S. An, B. Pourdeyhimi, S. S. Yoon and A. L. Yarin, *J. Mater. Chem. C*, 2013, **1**, 3491–3498.
17 H. Yoon, M. G. Mali, J. Y. Choi, M.-w. Kim, S. K. Choi, H. Park, S. S. Al-Deyab, M. T. Swihart, A. L. Yarin and S. S. Yoon, *Langmuir*, 2015, **31**, 3727–3737.
18 C.-C. Wang, J.-G. Chen, K.-C. Huang, H.-W. Chen, Y.-C. Wang, C.-Y. Hsu, R. Vittal, J.-J. Lin and K.-C. Ho, *J. Power Sources*, 2013, **239**, 496–499.
19 L. Xie, P. Brault, C. Coutanceau, J.-M. Bauchire, A. Caillard, S. Baranton, J. Berndt and E. C. Neyts, *Appl. Catal., B*, 2015, **162**, 21–26.
20 I. Lee, K.-Y. Chan and D. L. Phillips, *Appl. Surf. Sci.*, 1998, **136**, 321–330.
21 S. An, H. S. Jo, D. Y. Kim, H. J. Lee, B. K. Ju, S. S. Al-Deyab, J. H. Ahn, Y. Qin, M. T. Swihart, A. L. Yarin and S. S. Yoon, *Adv. Mater.*, 2016, **28**, 7149–7154.
22 S. J. Cho, C. Y. Neo, X. Mei and J. Ouyang, *Electrochim. Acta*, 2012, **85**, 16–24.
23 L. Giannuzzi and F. Stevie, *Micron*, 1999, **30**, 197–204.
24 J.-G. Lee, T. Nagase, H. Yasuda and H. Mori, *J. Appl. Phys.*, 2015, **117**, 194307.
25 S. Soltanian, R. Rahmanian, B. Gholamkhass, N. M. Kiasari, F. Ko and P. Servati, *Adv. Energy Mater.*, 2013, **3**, 1332–1337.
26 H. Wu, D. Kong, Z. Ruan, P.-C. Hsu, S. Wang, Z. Yu, T. J. Carney, L. Hu, S. Fan and Y. Cui, *Nat. Nanotechnol.*, 2013, **8**, 421–425.
27 B. Joshi, H. Yoon, H. Kim, M.-w. Kim, M. G. Mali, S. S. Al-Deyab and S. S. Yoon, *RSC Adv.*, 2015, **5**, 85323–85328.
28 S. S. Patil, M. G. Mali, M. S. Tamboli, D. R. Patil, M. V. Kulkarni, H. Yoon, H. Kim, S. S. Al-Deyab, S. S. Yoon and S. S. Kolekar, *Catal. Today*, 2016, **260**, 126–134.
29 J. G. Lee, D.-Y. Kim, J.-H. Lee, M.-w. Kim, S. An, H. S. Jo, C. Nervi, S. S. Al-Deyab, M. T. Swihart and S. S. Yoon, *ACS Appl. Mater. Interfaces*, 2016, **8**, 15406–15414.
30 M.-w. Kim, H. Yoon, T. Y. Ohm, H. S. Jo, S. An, S. K. Choi, H. Park, S. S. Al-Deyab, B. K. Min and M. T. Swihart, *Appl. Catal., B*, 2017, **201**, 479–485.
31 H. E. Swanson, E. Tatge and R. K. Fuyat, *Standard X-ray diffraction powder patterns*, Institute for Materials Research, Washington, D.C., 1953.
32 C. K. Gupta, *Chemical Metallurgy: Principles and Practice*, John Wiley & Sons, 2006.
33 D. Stauffer, *Phys. Rep.*, 1979, **54**, 1–74.
34 D. Stauffer and A. Aharony, *Introduction to Percolation Theory*, CRC Press, 1994.

